646

Q-Switched Neodymium-Doped Phosphate Glass Fiber Lasers

P. R. Morkel, K. P. Jedrzejewski, and E. R. Taylor

Abstract—**The operation of a short-pulse, Q-switched, Neodymium-doped fiber laser operating at 1.054 μm is described experimentally and theoretically. The laser is efficiently pumped with a single-stripe AlGaAs laser diode and emits >1 kW pulses. It is seen that due to high gain, short pulses with high energy extraction efficiency can be obtained. The feature of broad emission lines associated with rare-earth-doped glasses is exploited to demonstrate tunable, Q-switched operation over a 40 nm tuning range.**

I. Introduction

Q-SWITCHING of fiber lasers has followed a progressive development since the first reports of amplification in rare-earth-doped silica fibers [1]. The motivation behind their development has been an appreciation that the doped fiber configuration gives significant energy storage for relatively low levels of pump power and high gain to enable efficient energy extraction. In addition, the broad tunability associated with glass lasers indicates that the wavelength of operation of the laser is not predetermined but can be specified over a substantial range. These devices thus offer the possibility of high peak power, wavelength-tunable short pulse sources, with low power requirements, which will be suitable for use in a number of time-multiplexed optical sensor systems.

Initial Q-switched fiber lasers were formed with relatively low concentration germania/silica based fibers which necessitated rather long cavities. This limited the peak power output to a few Watts due the resultant low temporal gain [2]. Subsequent devices demonstrated with alumina/silica fibers capable of efficient operation at higher dopant concentrations enabled peak powers of 100 W with 15 ns duration to be demonstrated [3]. In this paper we show the operation of a diode-pumped device which shows a further order of magnitude increase in peak power output. This has been achieved as a result of number of factors, most particularly the use of a short, highly doped phosphate-glass fiber amplifier. The resultant high temporal gain necessitates the use of an electrooptic modulator to provide rapid switching and sufficient extinction.

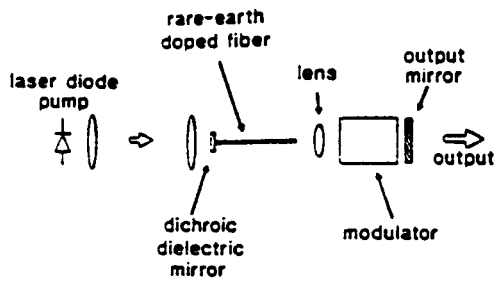

Fig. 1. General Q-switched fiber laser cavity schematic.

Q-switched operation of monomode fiber lasers can be theoretically described using a conventional semianalytical plane wave analysis [4] with a modification to account for the overlap between dopant, signal, and pump fields. Such an approach has been adopted in the description of Nd:YAG crystal fiber lasers [5]. Although this approach enables elegant description of the operation of a Q-switched laser, the effects of finite switching times are not readily included. For high gain systems such as fiber lasers the switch time may be comparable to the pulse build-up time for a number of modulator types and this will affect the output characteristics of the laser. In this paper we describe a numerical analysis which readily includes the effect of finite modulator switching time.

Fig. 1 shows a schematic Q-switched fiber laser cavity. A dichroic laser mirror which transmits pump light but reflects signal light is incorporated onto the end of a fiber amplifier. The other fiber end is terminated to minimize coupling of the 4% Fresnel reflection back into the fiber mode. A lens is used to focus or collimate the signal output from the fiber onto an output coupling mirror. A Q-switch modulator is incorporated in the air gap between the lens and the output coupling mirror to provide hold-off. With the modulator in the off state no extra loss is imparted to the cavity and CW lasing can take place when the fiber is longitudinally pumped. In the on state the modulator prevents laser action and enables the population inversion and single-pass gain to build up to a high value. Switching the modulator off enables laser action to build up rapidly to the extent that the gain is saturated to below the threshold value and a pulse is emitted.

Manuscript received July 23, 1992. This work was supported by a U.K. Government LINK program in collaboration with York Sensor Ltd.

P. R. Morkel and E. R. Taylor are with the Optoelectronics Research Centre, University of Southampton, Highfield, Southampton, SO9 5NH, UK.

K. P. Jedrzejewski was with the Optoelectronic Research Centre, University of Southampton. He is now with the Institute of Electronics Fundamentals, Warsaw University of Technology, Warsaw, Poland.

IEEE Log Number 9209973.

II. Theory

In this section the approach adopted in the theoretical analysis is described. The only major assumptions incorporated are a constant optical confinement factor in the waveguide and uniform axial photon density in the fiber amplifier. The former assumption is generally adopted in such analyses as its effect can only be accounted for by numerical integration transverse to the optical axis. It is ignored for the sake of simplicity and clarity. The latter assumption allows the fiber amplifier to be considered as a lumped element which obviates a requirement to perform a numerical integration along the fiber length. Although it is not readily apparent that this is the case in typical fiber laser configurations, a simple analysis shows the assumption to be reasonable for typical configurations.

Fig. 2 shows a simplified laser configuration schematic. A gain element G is incorporated between two mirrors, one of which is assumed to provide 100% reflection at the gain wavelength and the other an arbitrary reflection R. Intrinsic losses in the cavity between the gain medium and the output coupling mirror can be lumped into this reflectivity factor. Following an arbitrary signal P_o around the cavity under it is possible to determine the relative photon densities at different point in the cavity, in particular at points either end of the gain medium. Under CW or quasi-CW conditions we can see from self consistency arguments that $G^2R = 1$. Quasi-CW may be taken here to represent conditions under which time variations of the intracavity photon density are slow compared to the cavity round-trip time. The relative photon density at the output coupling mirror to that at the HR mirror is given by $(1 + R)/2GR$ or equivalently $(1 + R)/\sqrt{R}$. The photon density in the cavity is thus seen to vary for smaller values of R with the maximum photon density being located at the output coupling mirror end of the cavity. However, even for values of R as low as 30% it is seen that the photon density in this simplified cavity is constant to within 20%. Considering uncertainties in other laser parameters, this assumption is considered justified for most experimental conditions. In practice, we find experimentally that pulse durations as short as 2–3 times the cavity round-trip period can be obtained. Under these conditions the intracavity photon density cannot be considered as quasi-CW and this detracts from the assumption of axially uniform signal photon density somewhat. However, under these assumptions it will be seen that a very complete description of the operation of doped fiber lasers can be given, accounting for all the major effects. We believe the analysis to be sufficient to facilitate design and optimization of Q-switched fiber laser cavities, particularly considering the errors associated with specifying a number of parameters such as emission cross sections and refractive index profiles.

An effective modal area is used in the analysis to account for the overlap between signal and pump modes and the dopant distribution. For single mode pump and signal fields it is clear that choosing the core area from the refractive index profile will give an error which can become very large as the V-value of the fiber becomes successively smaller and the modes are propagated substantially in the cladding. In this analysis we determine the optical confinement using an overlap integral for Gaussian modes. The Gaussian approximation for the field distributions of fundamental modes is known to have a small error for V values (normalized frequencies) greater than unity [6].

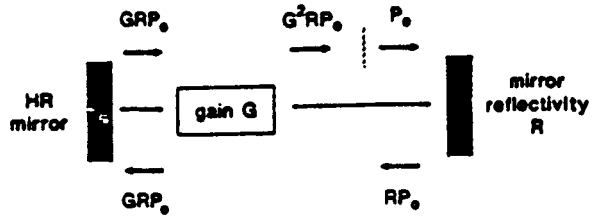

Fig. 2. Simplified laser configuration.

A. Confinement Factor

Referring to the simplified 4-level energy level diagram shown in Fig. 3, assuming a host medium with low background loss, under equilibrium conditions the small signal gain in a 4-level fiber laser medium can be written:

$$\frac{dP_s(z)}{dz} \cdot \frac{1}{P_s(z)} = \sigma_{32} \int_0^\infty S_s(r) N_T(r) \left[\frac{W_p(r, z)}{W_p(r, z) + \frac{1}{\tau_f}} \right] 2\pi r \, dr \tag{1}$$

where $W_p(r)$ is the radial variation of pump rate, $N_T(r)$ is the radial variation of rare-earth dopant concentration, and $S_s(r)$ is the normalized radial intensity distribution of the signal mode. σ_{32} is the emission cross section and τ_f is the upper level lifetime.

For

$$N_T(r) = N_T \quad r \le a_1$$
$$= 0 \quad r > a_1 \tag{2}$$

(i.e., a rectangular dopant distribution with radius a_1) and $W_p(r) \ll 1/\tau_f$ (small ground state depletion) then the signal gain can be expressed by:

$$\frac{dP_s(z)}{dz} \frac{1}{P_s(z)} = \frac{\sigma_{32} N_T \tau_f \sigma_{13} P_p(z)}{h\nu_p} \int_0^{a_1} S_s(r) S_p(r) 2\pi r \, dr \tag{3}$$

where σ_{13} is the pump absorption cross section. The pump absorption is given by:

$$P_p(z) = P_p(0) \exp\left(-\sigma_{13} N_T \left(\int_0^{a_1} S_p(r) \cdot 2\pi r \, dr \right) \cdot z \right) \tag{4}$$

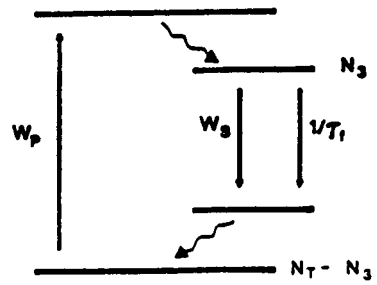

Fig. 3. General 4-level energy level diagram. Relaxation from the pump band and the lower laser level is assumed to be rapid such that only levels 1 and 3 are significantly populated.

Using

$$S_s(r) = \frac{2}{\pi\omega_s^2}\exp\left(-\frac{2r^2}{\omega_s^2}\right)$$

$$S_p(r) = \frac{2}{\pi\omega_p^2}\exp\left(-\frac{2r^2}{\omega_p^2}\right) \qquad \text{(Gaussian distributions)} \tag{5}$$

where ω_s, ω_p are the mode field radii of the signal and pump modes, respectively, and (4) for the pump absorption, then the single pass gain of the fiber can be determined from (3) to be:

$$\ln G = \int \frac{dP_s}{P_s} = \frac{\sigma_{32}\tau_f P_p^{abs}}{h\nu_p A_{eff}} \tag{6}$$

where P_p^{abs} is given by the difference between coupled and throughput pump power and A_{eff} is defined by

$$A_{eff} = \pi(\omega_s^2 + \omega_p^2)\frac{\left(1 - \exp\left(-\frac{2a_1^2}{\omega_p^2}\right)\right)}{2\left(1 - \exp\left[-2a_1^2\left(\frac{1}{\omega_s^2} + \frac{1}{\omega_p^2}\right)\right]\right)}. \tag{7}$$

Equation (7) compares with expressions obtained by Digonnet *et al.* [7] for an effective modal area which can be reduced to a form similar to (7) although without the term in parentheses in the denominator. We believe (7) can be tested in the limit of $a_1 << \omega_s, \omega_p$. In this case A_{eff}, defined by (7), reduces to $\pi\omega_s^2/2$, or the $1/e$ cross-sectional area of the signal *intensity* distribution. For a 4-level medium with negligible background loss, an independence of the effective modal area on the pump mode spot size is expected in this limit as the radial population inversion distribution become determined solely by the radial dopant distribution. Fig. 4 shows the variation of A_{eff} with V value for a Nd-doped fiber amplifier with a single-mode pump and lasing fields. A fiber numerical aperture of 0.2 has been used and the mode field radii determined from the core radius and fiber V value using the Marcuse formula [8]:

$$\frac{\omega}{a} \approx (0.65 + 1.619V^{-1.5} + 2.879V^{-6}). \tag{8}$$

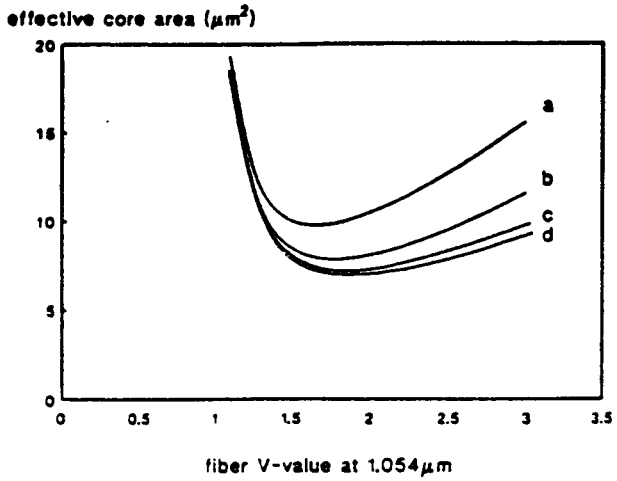

Fig. 4. Variation of effective core area with fiber V-value for pump at 810 nm and signal at 1.054 μm. Fiber NA = 0.2. Curves (a)-(c) represent dopant radius to core ratios of 1, 0.5, and 0.25, respectively. Curve (d) represents the inverse signal mode area given by $\pi\omega_s^2/2$ and represents the limit of dopant confinement to the core axis.

A number of rectangular dopant distributions are indicated in Fig. 4 with $a_1/a = 0.25$, 0.5 & 1. For fibers with differing numerical apertures, the effective core areas can be obtained by scaling the data in Fig. 4 by $NA^2/0.2^2$. The V-values indicated in Fig. 4 can be related to the fiber core radius, a, using $V = 2\pi \cdot a \cdot NA/\lambda$ or to the second mode cutoff wavelength of the fiber, λ_c, remembering that $V(\lambda_c) = 2.405$.

For Q-switching applications a minimum fiber length is desirable and $a_1 = 1$ is applicable (particularly for fibers manufactured by the rod-in tube technique). In this case, the peak gain (maximum confinement factor) occurs for $V \approx 1.7$–1.9 as previously identified [9]. Note however, that as the dopant is progressively confined to the core axis, the effective area becomes equivalent to that of the signal modal area. At an optimum V value of ≈ 1.7, for rare-earth dopant throughout the core region, the effective area is given by $A_{eff} \approx 0.7 \cdot \pi\omega_s^2$.

B. Laser Rate Equations

Fig. 3 shows a general 4-level energy-level diagram as applicable for Nd-doped fibers. Relaxation from the pump band into the metastable level is assumed to be rapid compared with the pump rate. This condition is generally well satisfied for such a glass host. In addition, relaxation from the lower energy level is assumed to be rapid compared with the stimulated emission rate. Care must be taken here as under Q-switched conditions the stimulated emission rate will in general be many orders of magnitude greater than under CW conditions. However, measurements of saturation fluences in similar glasses indicate a lower level lifetime <1 ns [10] and hence it is assumed negligible here. Constant signal photon density is assumed along the amplifier length such that the stimulated emission rate is constant along the amplifier. The photon density in the gap between the amplifier and the output coupling mirror is again assumed to be uniform and proportional to that

in the amplifier. Assuming negligible pump excited-state absorption and pump background loss, a rate equation for the upper energy level, for constant pumping, can be written:

$$\frac{\partial N_2(z,t)}{\partial t} = \frac{d\phi_p(z)}{dz}\eta\frac{c}{n} - \frac{N_2(z,t)}{\tau_f} - \frac{c}{n}\phi_s(t)\sigma_{32}N_2(z,t) \tag{9}$$

where η represents a pump quantum efficiency, $\phi_p(z)$ the pump photon density, ϕ_s the signal photon density, τ_f the metastable level lifetime and σ_{32} the stimulated cross section. n is the refractive index of the fiber core (≈ 1.5).

For uniform signal photon density in the fiber given by $\phi_s(t)$ and uniform photon density in the air gap given by $\phi_s(t)/n$, then the rate of change of the photon density can be written:

$$\frac{d\phi_s(t)}{dt} = c\sigma_{32}\phi_s(t)\frac{\int N_2(z,t)\,dz}{nl_1 + l_2} - \frac{\phi_s(t)}{\tau_c(t)} \tag{10}$$

where l_1 is the doped fiber length and l_2 is the amplifier-mirror gap length.

Equation (10) gives the rate of variation of signal photon density in the cavity in terms of the integral population inversion along the cavity length. This integral can be obtained from (9). For partial derivatives which are continuous, (9) can be integrated such that:

$$\frac{d\left[\int N_2(z,t)\,dz\right]}{dt} = \eta\frac{c}{n}\int d\phi_p(z) - \frac{\int N_2(z,t)\,dz}{\tau_f} - \frac{c}{n}\phi_s(t)\sigma_{32}\left[\int N_2(z,t)\,dz\right] \tag{11}$$

or in terms of absorbed pump power (11) becomes

$$\frac{d\left[\int N_2(z,t)\,dz\right]}{dt} = \frac{\eta P_p^{abs}}{h\nu_p A_{eff}} - \frac{\int N_2(z,t)\,dz}{\tau_f} - \frac{c}{n}\phi_s(t)\sigma_{32}\left[\int N_2(z,t)\,dz\right]. \tag{12}$$

Equations (10) and (12) are thus expressed in terms of the integral population inversion over the amplifier length and hence simultaneous solution of these equations only involves numerical calculations in time. Note that (10) includes a general time dependent decay rate $\tau_c(t)$ which can be used to model the effects of a modulator with finite switch time. The cavity lifetime will be given by:

$$\tau_c(t) = \left[-\frac{2(nl_1 + l_2)}{c}\cdot\frac{1}{ln(1-T) + ln(1-L_i) + ln(1-L_s(t))}\right] \tag{13}$$

where T is the output coupling, L_i is the cavity intrinsic losses, and $L_s(t)$ is the modulator loss.

For simplicity $L_s(t)$ can be modeled as an exponentially decaying function (which is seen to approximate the measured characteristic) whereby:

$$L_s(t) = L_s(0)\exp\left(-\frac{t}{\tau_s}\right) \tag{14}$$

where τ_s is the switching time and $L_s(0)$ is the loss of the switch in the on state.

For constant pumping, the initial integral inversion is given by

$$\int N_1^{init}\,dz = \int N_1'\,dz \cdot \exp\left(-\frac{T_1}{T_f}\right) + \frac{P_p^{(abs)}\eta T_f}{h\nu_f A_{eff}}\cdot\left(1 - \exp\left(-\frac{T_1}{\tau_f}\right)\right) \tag{15}$$

where T_1 is the time between Q-switched pulses and $\int N_1'\,dz$ is the integral inversion remaining just after the Q-switched pulse is emitted.

or

$$\int N_1^{init}\,dz = \frac{nl_1 + l_2}{c\tau_c\sigma_{32}}. \tag{16}$$

Whichever of (15) or (16) is the larger.

Equation (15) relates to the maximum possible inversion attainable for the pump power available and (16) relates to the inversion at CW lasing threshold. If the switch extinction is insufficient to prevent prelasing then (16) will determine the maximum inversion, otherwise (15) holds. The first term on the right-hand side of (15) relates to the remaining inversion from the previous Q-switch pulse and is generally only significant for low pump powers or high repetition rates where the energy extraction is substantially less than unity. Finally the output power of the laser can be determined from the signal photon density in the cavity and the output coupling rate:

$$P_{out}(t) = \phi_s(t)h\nu_s A_{eff}R_{oc}\left(l_1 + \frac{l_2}{n}\right). \tag{17}$$

where R_{oc} is defined by:

$$R_{oc} = -\frac{c}{2(nl_1 + l_2)}ln(1-T) \tag{18}$$

C. CW Characteristics

The above rate equations can conveniently be manipulated to give the CW characteristics of the fiber laser. Under CW conditions the signal photon density and integral population inversion become constant and (10) and (12) can be solved in equilibrium to give analytical expressions for the laser output power. Such an analysis is of interest here as it enables parameters such as the intrinsic cavity losses to be determined.

Equation (10) can be used to give the integral population inversion in the cavity above threshold:

$$\int N_2(z)\,dz = \frac{nl_1 + l_2}{c\tau\sigma_{32}} \tag{19}$$

incorporating this in (12) gives:

$$\phi_s(P_p) = \frac{\tau_c \eta P_p^{abs} n}{A_{eff} h\nu_p (nl_1 + l_2)} - \frac{n}{c\sigma_{32}\tau_f} \tag{20}$$

where P_p^{abs} represents absorbed pump power in the fiber which is taken to be time invariant. Equating the terms on the rhs of (20) gives the laser threshold and differentiating wrt P_p^{abs} gives the laser slope efficiency above threshold.

Incorporating the cavity output coupling rate from (18), the cavity lifetime from (13) and expressing the output in terms of power we get for the slope efficiency:

$$\frac{dP_s}{dP_p^{abs}} = \eta \cdot \frac{\nu_s}{\nu_p} \cdot \frac{ln(1 - T)}{ln(1 - T) + ln(1 - L_i)}. \tag{21}$$

Equation (21) which has been simply derived is seen to give results within 6% of a conventional large output coupling Rigrod analysis (see e.g. [4]) for $L_i < 70\%$ and $T < 95\%$ which covers most conceivable experimental conditions. For $L_i < 50\%$ and $T < 75\%$ the difference becomes less than 2%.

III. Experimental Evaluation of Parameters

The important parameters required for modelling of Q-switched devies can be determined from evaluation of CW laser characteristics and waveguide parameters. Initially we describe the signal mode spot size measurement method. The characterizations were performed using various lengths of the doped fiber. The fiber consisted of a core of 1 wt% Schott LG750 glass in a cladding of similar undoped phosphate glass. The rod-in-tube fabrication technique has been described elsewhere [11].

A. Fiber Mode Field Diameters

In order to determine the signal mode spot size a short length of the neodymium-phosphate fiber was cleaved and pumped with light at 812 nm from a laser diode. Fluorescence from the fiber end was detected with a 300 μm diameter InGaAs photodetector in the far field at a range of 34 mm from the fiber end. An RG1000 filter was used to block pump throughput and 900 nm emission. Mechanically scanning the detector across the far field pattern confirmed single mode emission and enabled the field spot size to be measured as 4.9 $\pm$ 0.3 mm. Using standard gaussian beam expressions this implied a fiber mode field radius at 1.054 μm of 2.3 $\pm$ 0.15 μm. For the pump light a mode field radius in the fiber of 1.8 $\pm$ 0.11 μm was determined. These compare with the fiber core radius of 1.7 $\pm$ 0.1 μm.

B. Fluorescence Characteristics

Pulsing the pump beam enabled a 1/e fluorescent lifetime of 305 $\pm$ 5 μs to be measured. Note that this compares with approximately 350 μs we have measured for the bulk LG750 material (which agrees with the glass manufacturers data [12]). Care was taken to prevent superfluorescence in this measurement which would reduce the lifetime. Clearly the fiber pulling process varies the rare-earth environment to a certain degree. The fluorescence spectrum was essentially unchanged from that of the bulk material. Fig. 5 shows a spectrum obtained at low pump power.

C. Emission Cross Section

The emission cross section of Nd^{3+} ions in the fiber was determined by measuring the fiber gain. This was done by determining the power required to reach laser threshold for a known cavity loss. This was performed by evaluating the laser threshold for a 50 mm length of fiber potted in a 2 mm outer diameter capilliary. Careful polishing of the ends of the capilliary left 4% Fresnel reflection feedback at each end. Using a single-stripe 100 mW laser diode pump source (SDL5411) an incident threshold power of 30 mW was measured. This was very similar to a pump power value of 28 mW separately measured for a 10 cm length of the bare fiber with inspected, cleaved fiber ends providing the optical feedback.

It was not possible to determine the launched pump power fraction for the doped fiber directly due to the high concentration of rare-earth dopant. However, replacing the doped fiber with an undoped silica fiber with nominally similar waveguide characteristics enabled the launched power fraction to be estimated. The undoped fiber had a pump mode field diameter within 15% of that of the doped fiber and under such circumstances one might expect very similar launch efficiencies. A launched to incident pump power ratio of 52% was measured which compares very favorably with other AlGaAs laser diode sources.

Using the 52% launch efficiency value the laser threshold powers were determined to be 15.6 mW and 14.6 mW for the capilliary and bare fiber, respectively. The single-pass gain required to reach threshold under these conditions is 14.0 dB. Taking into consideration a possible error in the launch efficiency we determined the gain of the fiber to be 0.95 $\pm$ 0.10 dB/mW.

Using (6) and (7) the emission cross section of the fiber can be determined from the gain of the fiber. Assuming uniform dopant distribution across the core area (justified for such fibers), the effective core area can be determined from the measured spot sizes and knowing the core radius using (7). Using $\omega_s = 2.2$ μm, $\omega_p = 1.8$ μm, the small signal effective core area is calculated to be 11.4 $\pm$ 1.5 μm^2. Using this value in (6) along with the measured gain parameter and the known fluorescent lifetime we get $\sigma_{21} = 2.0 \pm 0.25 \times 10^{-20}$ cm^2. The authors are aware that this value is less than that determined for the bulk material [12]. An obvious possible source of discrepancy from this analysis is the use of a dummy fiber to determine the doped fiber launch efficiency. However any error incurred by this

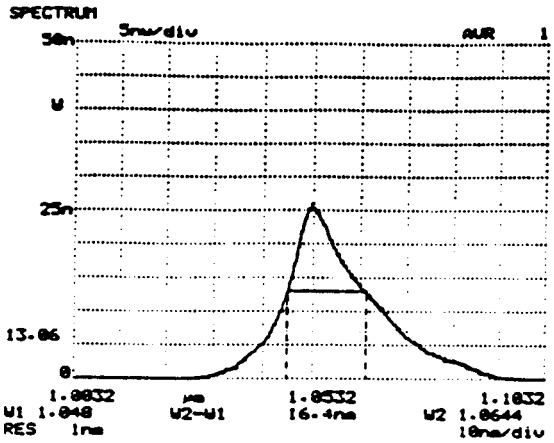

Fig. 5. Fibre fluorescence spectrum obtained by pumping fiber with low power at 812 nm (< 1 mW).

is unlikely to be greater than ≈ 10% and hence it does not explain the factor of 2 difference in emission cross sections. We believe that it is possible that the cross section in the fiber is significantly different to that of the bulk material. The observation of a variation in fluorescent lifetime between the two media suggests that the rare-earth environment is affected somewhat. It is possible that for such small core dimensions an effect associated with the core/cladding interface will affect substantially the whole doped core. It should be noted however that the measured cross section is approximately a factor of 2 higher than those of a number of Nd:silica fibers from various manufacturers and higher than that measured previously for a Nd-doped phosphate glass fiber [7].

D. Cavity Losses

The intrinsic cavity losses associated with the Q-switch laser configuration can be determined by comparing the laser slope efficiencies obtained with various values of output coupling. These losses consist of Fresnel reflection losses at the fiber to air interface, losses associated with the intracavity lens and losses at the pump input mirror due to imperfect polishing or coating. A laser configuration similar to that shown in Fig. 1 was used to determine the laser slope efficiencies. One of the 25 mm end-polished capilliaries, containing the phosphate fiber, was used as the laser gain medium. A multilayer dielectric coating was applied to one end of the capilliary to form the pump input mirror. The coating showed >99% reflectivity at 1054 nm with 94% transmission at 812 nm. At the other capilliary end a 3 mm × 3 mm section of 1 mm thick silicate microscope slide was bonded to the capilliary using index matched U.V. curing epoxy. The purpose of this was to displace the 4% Fresnel reflection from the end of the waveguide in order to prevent feedback. Such a configuration was calculated to provide < −40 dB reflection into the fiber core. An intracavity lens of focal length 4.5 mm was used to collimate or focus the fiber output onto the output coupling mirror which provided feedback into the fiber. The laser characteristics were determined by varying the laser diode drive current and monitoring the fiber laser output with a calibrated large area Ge photodiode power meter. Measurements were made with and without the modulator in the cavity.

Using (21), the intrinsic loss of the cavity (assumed constant) can be determined by evaluating the slope efficiencies obtained with differing values of output coupling. From (21) we get:

$$L_i = 1 - \exp\left(\frac{\ln(1 - T_1)\ln(1 - T_2)(S_2 - S_1)}{\ln(1 - T_2)S_1 - \ln(1 - T_1)S_2}\right) \quad (22)$$

where S_1, S_2 are the differential slope efficiencies obtained with output couplers T_1 and T_2, respectively.

Using output coupling mirror transmission of 30%, 50%, and 70%, the slope efficiencies measured with respect to incident pump power were 13.4%, 17.1% and 19.3%, respectively. Note that it is not necessary to know the coupled pump fraction in this evaluation. Incorporating these values we get $L_i = 0.24 \pm 0.02$. Incorporating the Pockels cell Q-switch gave $L_i = 0.32 \pm 0.02$.

E. Pump Quantum Efficiency

Knowing the cavity intrinsic losses and the absorbed pump power it is then possible to determine the pump quantum efficiency for such fibers. The measured slope efficiencies for the laser with output mirror reflectivities of 30%, 50%, and 70%, with respect to absorbed pump power, were 61 ± 6%, 54 ± 5%, and 42 ± 4%, respectively. Using these values with the intrinsic loss figure, already determined, we get from (21), $\eta = 0.97 \pm 0.10$. Hence we see that the majority of absorbed pump photons give rise to excited ions.

F. Summary

Using a number of techniques we have been able to determine all the parameters essential for modeling of Q-switched laser devices using the expressions derived in the previous section. Of the material parameters it is interesting to note that the fluorescence lifetime of the doped fibers is less than that of the bulk material as is the emission cross section.

IV. Q-Switched Laser Modeling

In this section general results of the numerical simulations are presented. The intention has been to provide an insight into the method of operation of Q-switched fiber laser devices by examining the dependence of the laser output on one of a number of parameters, such as switch time, switch loss, etc. This can be done by examining the effect of variation of one parameter on an otherwise "perfect" laser system where the Q-switching process is not affected by any of the other parameters. This approach has been adopted here as it enables insight into the effect of individual parameters and provides a degree of generality. All of the fiber parameters are taken to be the values determined in Section III with a resonator length corresponding to the laser described in the section on experimental

results. In a real system the dependencies are not independent of each other and the variation of one parameter has the effect of varying the dependence on another parameter. However, it is often the case that real systems are limited primarily by one of the variable parameters and hence this approach is a valid and useful way to investigate the characteristics of such a system.

Initially in this section an idealized laser is considered with a perfect switch. Such a switch would show negligible transmission in the on state and unity transmission in the off state with negligible switching time in between. This data therefore relates to the maximum possible performance attainable. The loss values modeled in each case refer to $(T + L_i - TL_i)$ and the generated energy relates to the intracavity energy. The useful output energy will depend on the relative magnitudes of T and L_i in each case. For $L_i << T$, then essentially all the generated energy will be available at the laser output. Subsequently, the Q-switched laser dependencies on switch time and switch loss are considered.

In the modeling, only an integration over time is required and in the following data a time step of 5–20 ps was used.

Parameters used in the following simulations were:

Pump power = 20 mW (for fixed pump power evaluations)

Pump wavelength = 812 nm

lasing wavelength = 1054 nm

Repetition rate = 400 Hz (for fixed repetition rate evaluations)

Fiber length = 2.5 cm

Total resonator length = 10.5 cm.

A. Pump Power Dependence

For an ideal switch and at low repetition rate, the variation of generated Q-switch pulse energy and pulse duration with pump power is shown in Fig. 6. Cavity loss of 50% is indicated. For zero cavity intrinsic loss then these values refer to the transmission of the output coupling mirror. Above 5 mW pump power essentially complete energy extraction is effected and the characteristics become linear. The pulse duration is seen to tend to a limit given by the cavity photon lifetime [4].

B. Switch Time Dependence

The dependence of the laser output characteristics on the switch time are described in this section. In the analysis a source or seed signal is required to initiate the build up of a Q-switched laser pulse. This seed is given by the spontaneous emission which is captured and guided into the fiber mode. A capture fraction (C) of 0.3% was used in the analysis, determined from the numerical aperture of the fiber [13]. In fact the results are not highly sensitive to the value of C chosen and variations or an order of

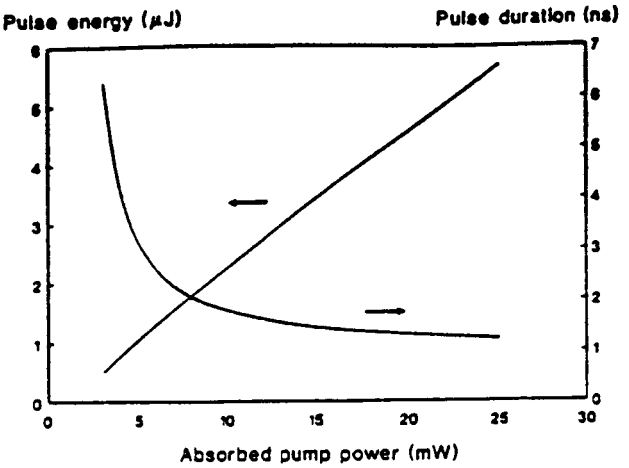

Fig. 6. Theoretical pulse energy and duration vs. pump power for "ideal" switch. Cavity loss 50%.

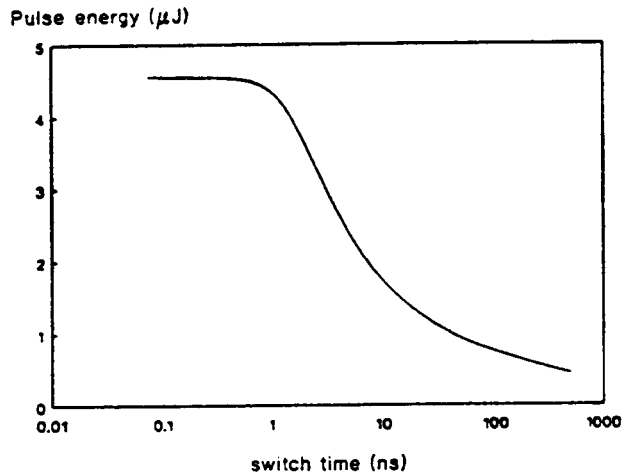

Fig. 7. Theoretical pulse energy vs. switch time for 50% loss cavity, 20 mW pump power at 810 nm & high-loss switch ($L_i > 0.9999$).

magnitude or more are required in order to observe an appreciable difference.

Fig. 7 shows the variation of generated pulse energy with switch time for a cavity with 50% loss. The switch hold-off is assumed to be sufficient to prevent prelasing and an absorbed pump power of 20 mW is used. It is seen that above 1 ns switch time the output decreases sharply. Such a switch time is generally not achievable using acoustooptic modulators and indicates that electrooptic devices are required. Note that the output energy drops to approximately half its maximum value for $\tau_s \approx 5$ ns. The lost energy is dissipated by the switch. The requirement for rapid switching in order to obtain the maximum efficiency is seen to be due to the high temporal gain exhibited in the laser. For a laser length of 11 cm with 20 dB single-pass gain, the net temporal gain is seen to exceed 40 dB/ns. Under these conditions the pulse build-up time is a few nanoseconds and the switch time must be less than this in order to prevent loss.

C. Switch Loss Dependence

The degree of loss imparted by an intracavity switch in the on state is critical in determining the pulse character-

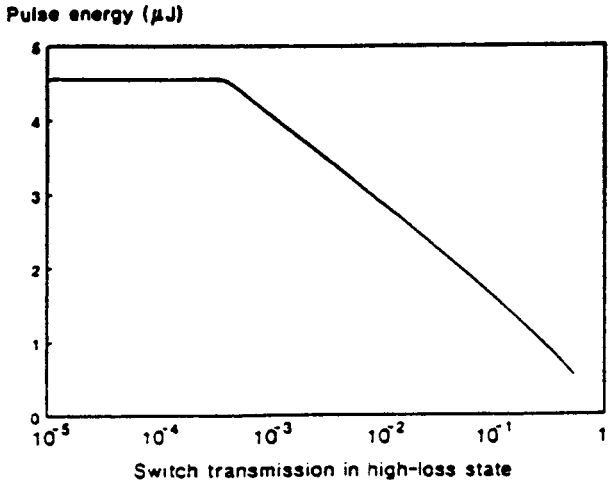

Fig. 8. Theoretical pulse energy vs. switch loss in ON (high loss) state. Pump power 20 mW at 810 nm, cavity loss 50%, switch time < 1 ns.

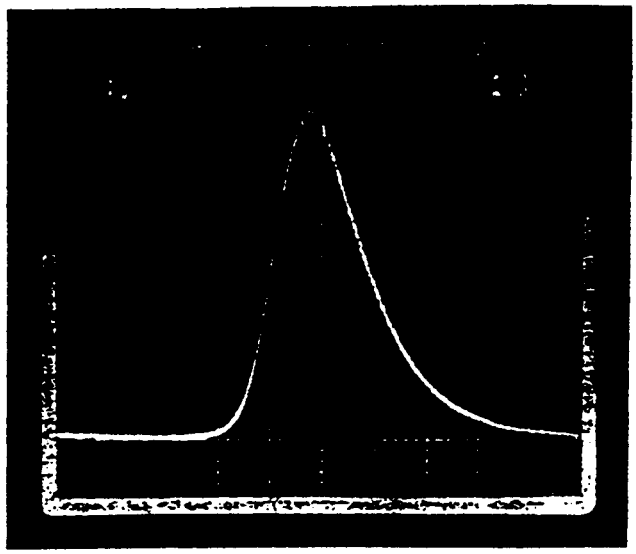

Fig. 9. Typical Q-switched pulse obtained at maximum pump power (22 mW). Peak power 1.06 kW, duration 2 ns.

istics of a high gain laser. If the switch is of insufficient holdoff to prevent lasing then the stored energy in the laser will be compromised and the output pulses will be of reduced energy. As the stored energy becomes clamped at laser threshold, increasing the pump power will result in pulses of no greater energy at the laser output. Fig. 8 shows the simulated switch holdoff characteristic where the laser output pulse energy is plotted against the transmission of the switch in the on state, on a logarithmic scale, for a cavity with 50% loss. Here the switch time has been assumed to be sufficiently rapid such that it does not affect the output characteristics. Above a certain threshold ($L_s(0) \approx 0.9995$) the energy characteristic is seen to reduce approximately linearly.

V. Experimental

An experimental configuration as shown schematically in Fig. 1 was used. A 25 mm coated capilliary amplifier was used as described in Section III. An intra-cavity lens of focal length 4.5 mm (Newport FL40B) was used to collimate or focus the fiber output onto a 30% reflection mirror which provided the laser output and round-trip feedback. For the pump power available 30% reflection gave higher peak power pulses than either 10% or 50% reflection mirrors which were also available. A compact electrooptic integrated Q-switch was used to modulate the cavity loss. This device (Gsänger IQS-7) has dimensions of 35 mm diameter × 50 mm length and incorporates a thin film polarizer with an axis aligned at 45° to the axes of a KD*P 1/4 wave Pockels cell. The overall cavity length (10.5 cm) was dominated by the length of the Q-switching element. A 100 mW single-stripe laser diode operating at 812 nm (SDL5411) was used as the pump source and was coupled into the fiber with approximately 1:1 imaging of the laser diode onto the fiber core using two 8.6 mm objective lenses (Newport FL20). The Q-switch was driven was 3.4 kV pulses at varying repetition rate using an avalanche-transistor-chain driver. The output of the Q-switched laser was detected with a calibrated reverse biased 300 μm diameter InGaAs photodetector and a high speed (7 GHz) fiber coupled InGaAs detector. Calibrated inconel neutral density filters were used in tandem to limit the power incident on the detectors. Pulses were observed using a 1 GHz oscilloscope.

Fig. 9 shows a typical Q-switched pulse obtained with approximately 22 mW absorbed pump power and at sub 1 kHz repetition rate. The peak power is 1.06 kW ± 0.05 and the duration 2 ns. Note that this pulse duration is comparable with that of the round trip propagation delay of the resonator (0.8 ns). The laser output was seen to be unaffected by the rotational orientation of the Q-switch with respect to the optical axis implying that birefringence effects in the fiber were of no consequence. No modal ripple was observed with the cavity optimally aligned due to the large number of longitudinal modes present in the measured 2 nm FWHM laser spectrum.

Fig. 10 shows the variation of output energy and pulse duration (at sub 1 kHz repetition rate) with the absorbed pump power. The pulse energy was taken to be given by the peak power multiplied by the FWHM pulsewidth. The threshold pump power is seen to be only 2–3 mW and thus the laser can be operated at ≈ 10 times threshold. The pulse duration is seen to be limited to around 2 ns, a value higher than that indicated in Fig. 6. Additionally, for a pump rate ≈ 10× threshold, an analysis as given by Siegman [4] indicates that a pulse duration approximately 1.5 times the cavity photon lifetime is to be expected. In agreement with Fig. 6 this indicates an expected pulse duration of ≈ 1 ns. Clearly, a discrepancy exists here the origin of which is likely to be due to the assumption of uniform photon density in the cavity. For predicted pulse durations comparable with the round trip period the photon density in the cavity will not be uniform and this may prevent shorter pulses from being expected. Similarly, an assumption of a cavity lifetime longer than the round trip period is implicit in a Siegman type analysis [4]. Both assumptions are equivalent.

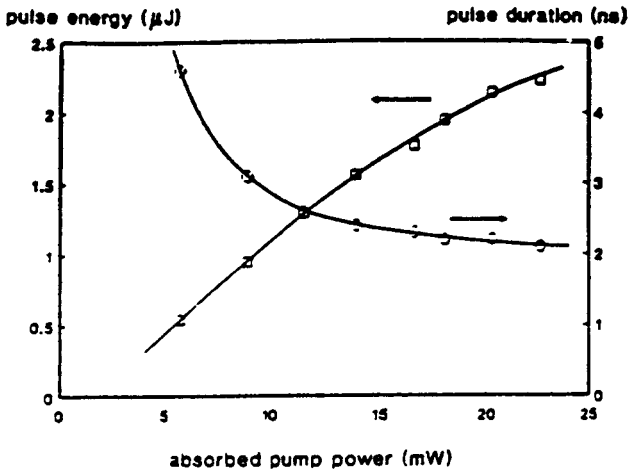

Fig. 10. Experimental variation of Q-switched fiber lasing pulse energy and duration with pump power at low repetition frequency (400 Hz).

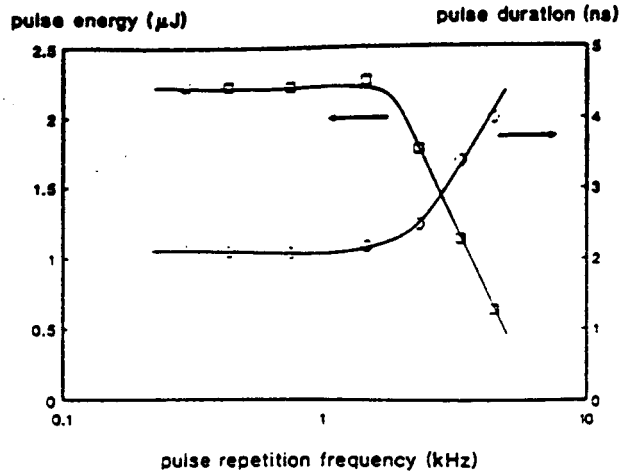

Fig. 11. Experimental variation of Q-switched fiber laser pulse energy and duration with repetition frequency at maximum pump power (22 mW).

Fig. 11 shows the variation of pulse energy and pulse duration as a function of repetition frequency at maximum pump power. Above ≈ 1.8 kHz, lower-energy, longer-duration pulses are observed.

A. Modeling the Experimental Conditions

Using all the parameters determined in Section III, the performance of the experimental Q-switched laser can be modeled. The electrooptic switch characteristics were experimentally determined optically by measuring the switching time of a CW signal at 1.053 μm. The switching characteristic was seen to approximate an exponential decay with ≈ 7 ns decay time. Additionally, the modulator was seen to provide sufficient extinction to prevent lasing under the highest pump power conditions in the Q-switched laser configuration and thus the initial switch loss could be taken to be >0.9999. Fig. 12 shows the predicted performance with respect to pump power incorporating the pertinent experimental parameters. These were $L_i = 0.32$, $\tau_s = 7$ ns, $T = 70\%$. Fig. 12 shows a maximum output of approximately 2.3 μJ with a pulse duration of ≈ 0.8 ns for 22 mW absorbed pump power. The pulse energy agrees well with that of the experimental data shown in Fig. 10. However, the pulse duration is shorter as discussed previously. Fig. 13 shows the modeled repetition rate characteristic for 20 mW pump power which compares favorably with the experimental data shown in Fig. 11.

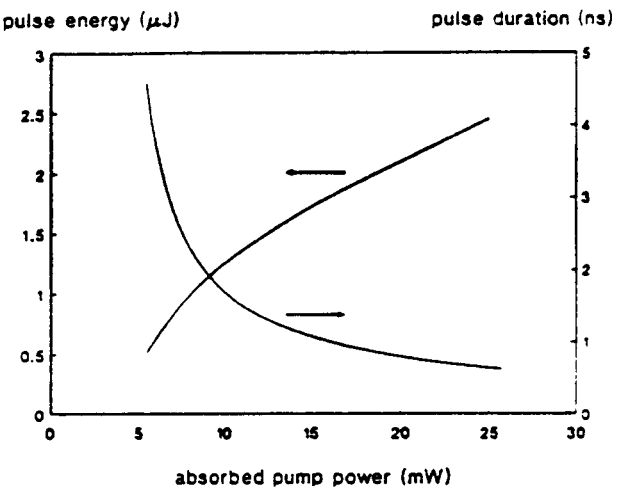

Fig. 12. Theoretical modeling of pulse energy and duration vs. pump power for the experimental conditions. Repetition frequency 400 Hz.

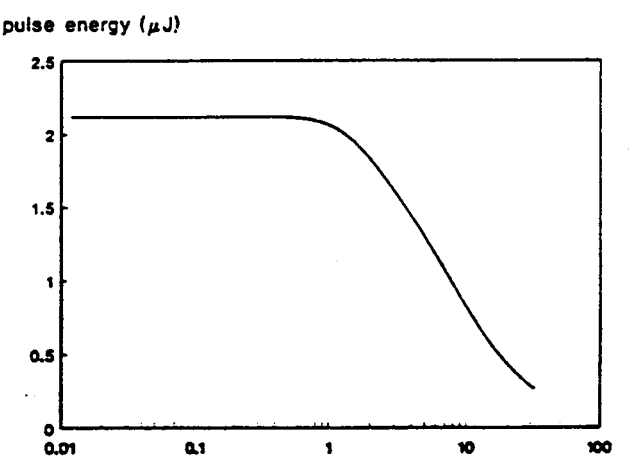

Fig. 13. Theoretical modeling of pulse energy vs. repetition rate for the experimental conditions. Pump power 20 mW.

B. Tunable Operation

A tunable Q-switched laser was constructed as shown schematically in Fig. 14. The same 25 mm fiber amplifier and modulator were used, as in the untunable configuration, and a 12001/mm grating, blazed at 1 μm, was used as the dispersive feedback element. A pellicle beamsplitter was used as the output coupling element. The beamsplitter had a measured 20.3% output coupling at 45° incidence although another output was generated by light returning from the grating. The total cavity length in this case was 15 cm. Fig. 15 shows the pulse output energy and duration, obtained at low repetition rates, at the maximum absorbed pump power of 22 mW. For each wavelength the spectral width was measured to be instrument limited at 0.1 nm. The pulse energy characteristic re-

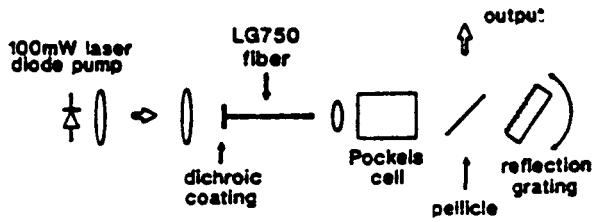

Fig. 14. Tunable, Q-switched fiber laser schematic.

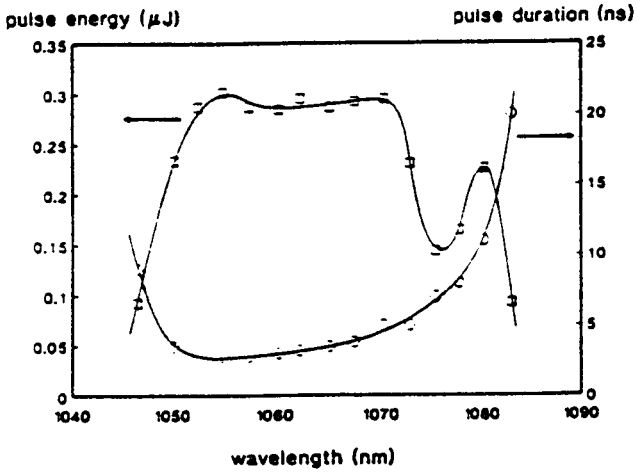

Fig. 15. Experimental tunable Q-switched results. Pulse energy and duration vs. wavelength. Spectral width <0.1 nm throughout, pump power 22 mW, repetition rate 400 Hz.

mained fairly flat over the wavelength range 1052–1072 nm and a secondary peak appeared at 1080 nm. The peak power characteristic broadly follows the shape of the fluorescence spectrum shown in Fig. 5 and coupled with an increase in pulse duration at longer wavelengths, this produces the peak in the characteristic at 1080 nm. A minimum pulse duration of 3 ns was obtained at 1053 nm corresponding the peak gain wavelength. Pulses of similar energy were coupled out of the resonator away from the detector so the total energy output is approximately double that shown in Fig. 15. A similar repetition frequency dependence to that shown in Fig. 11 was obtained.

VI. Discussion and Summary

In this paper we have described the implementation and operation of a Q-switched fiber laser using multicomponent Nd-doped phosphate glass as the amplifying medium. Techniques to characterize the waveguide and laser parameters have been described. Of particular interest here is the measurement of a fluorescence lifetime which is less than that of the bulk material and an emission cross section which is less than published values for the bulk material. However, the fiber still shows high gain of 0.95 ± 0.1 dB/mW at 1.053 μm, a value 2–3 times that of typical Nd-doped silica fibers. It is this feature, coupled with the relatively high dopant concentration which allows high temporal gain (measured in dB/ns) to be obtained making the fiber highly suitable for generation of short Q-switched pulses for low levels of pump power. Theory describing the operation of Q-switched fiber lasers is presented. Under the assumption of spatially uniform signal photon density in the cavity it becomes possible to readily investigate the effect of variation of a number of parameters on the laser output. Only numerical integration over time is required and thus the computational time is minimal. From the analysis it is apparent that for a system showing such high temporal and spatial gain, a highly specified modulator is necessary. Ideally < 1 ns switch time with > 30 dB extinction is required and this implies the use of an electrooptic modulator.

Experimentally, we have demonstrated the generation of 2.2 μJ, 2 ns duration pulses at up to 2 kHz repetition rate with only 22 mW of absorbed pump at 812 nm from a laser diode. Such a laser source is ideally suited for use in distributed fiber sensors such as temperature sensors [14] due to the high spatial resolution that can be obtained. We are confident that optimization of the fiber dopant concentration and development of a more compact modulator will enable ≈ 1 ns pulses to be readily obtained for similar values of pump power. Modeling the laser using the theory and incorporating measured parameters gave a very close match for the energy per pulse. However, the pulse duration was experimentally observed to exceed the theoretical values. The cause of the disrepancy could either have been due to less than expected gain due to a nonlinearity in the gain (the fiber gain characteristics were determined at low levels of pump power) or to a breakdown of the theory for predicted pulse durations comparable to the cavity round trip period. The latter characteristic results in non-uniformity of the photon density in the cavity. This is the most likely cause of the discrepancy. It should be noted that other traditional Q-switching theories also break down in this limit. To accurately describe operation of Q-switched lasers under such high gain conditions a complex and time consuming numerical integration over length and time must be performed. It is interesting to note empirically however that the experimental pulse durations are a constant 1.35 ns (or 1.65 round trip periods) greater than the theoretical data. Incorporating this factor gives a very close match between Figs. 10 and 12.

In addition, the feature of broad emission lines has been exploited to demonstrate tunable, Q-switched operation over a 40 nm range around 1060 nm. < 10 ns pulse durations could be obtained over a 30 nm range. Such wavelength diversity will be attractive for use in multichannel sensor systems.

Acknowledgment

The authors wish to acknowledge Dr. A. H. Hartog of York Sensors, Chandlers Ford, U.K. for fruitful discussions.

References

[1] R. J. Mears, L. Reekie, S. B. Poole, and D. N. Payne, "Neodymium-doped silica single-mode fibre lasers," *El. Lett.*, vol. 21, no. 17, pp. 738–740, 1985.

[2] I. P. Alcock, A. C. Tropper, A. I. Ferguson, and D. C. Hanna, "Q-switched operation of a neodymium-doped monomode fibre laser," *El. Lett.*, vol. 22, no. 2, pp. 84–85, 1986.
[3] W. L. Barnes, P. R. Morkel, M. C. Farries, L. Reekie, and D. N. Payne, "Q-switching in fibre lasers," in *Proceedings of the SPIE Fiber Laser Sources and Amplifiers Conference* (Boston, 1988), SPIE, vol. 1171, pp. 298–308.
[4] A. E. Siegman, *Lasers*. Oxford, U.K.: Oxford University Press, 1986.
[5] C. J. Gaeta, M. J. F. Digonnet, and H. J. Shaw, "Pulse characteristics of Q-switched fiber lasers," *Journal of Lightwave Technology*, vol. LT-5, no. 12, pp. 1645–1651, 1987.
[6] A. W. Snyder and J. D. Love, Optical Waveguide Theory. London: Chapman & Hall, 1983.
[7] M. J. F. Digonnet, K. Liu, and H. J. Shaw, "Characterisation and optimisation of the gain in Nd-doped single-mode fibers," *IEEE Journal of Quantum Electronics*, vol. 26, no. 6, pp. 1105–1110, 1990.
[8] D. Marcuse, "Loss analysis of single-mode fiber splices," *Bell Systems Technical Journal*, pp. 703–718, 1977.
[9] M. J. F. Digonnet and C. J. Gaeta, "Theoretical analysis of optical fiber laser amplifiers and oscillators," *Applied Optics*, vol. 24, no. 3, pp. 333–342, 1985.
[10] S. M. Yarena and D. Milam, "Gain saturation in phosphate laser glasses," *IEEE Journal of Quantum Electronics*, vol. QE-18, pp. 1941–1946, 1982.
[11] E. R. Taylor, D. J. Taylor, L. Li, M. Tachibana, J. E. Townsend, J. Wang, P. Wells, L. Reekie, P. R. Morkel, and D. N. Payne, "Application specific optical fibres manufactured from multicomponent glasses," in *Proceedings of the 1989 Materials Research Society Symposium*, vol. 172, pp. 321–327, Boston, MA, 1989.
[12] Schott laser glass product data.
[13] A. H. Hartog and M. P. Gold, "On the theory of backscattering in single-mode optical fibers," *Journal of Lightwave Technology*, vol. LT-2, no. 2, pp. 76–82, 1982.
[14] A. H. Hartog, "Recent advances in fiber optic distributed sensing systems," in *Proceedings of Optical Fiber Sensors Conference (OFS'92)*, Monterey, CA, paper Th1.1, pp. 246–249, 1992.

P. R. Morkel, photograph and biography not available at the time of publication.

K. P. Jedrzejewski, photograph and biography not available at the time of publication.

E. R. Taylor, photograph and biography not available at the time of publication.